IEEE Photonics Journal
An IEEE Photonics Society Publication

Negative Power Penalties of Optical OFDM Signal Transmissions in Directly Modulated DFB Laser-Based IMDD Systems Incorporating Negative Dispersion Fibers

Volume 2, Number 4, August 2010

X. Zheng
X. Q. Jin
R. P. Giddings
J. L. Wei
E. Hugues-Salas
Y. H. Hong
J. M. Tang

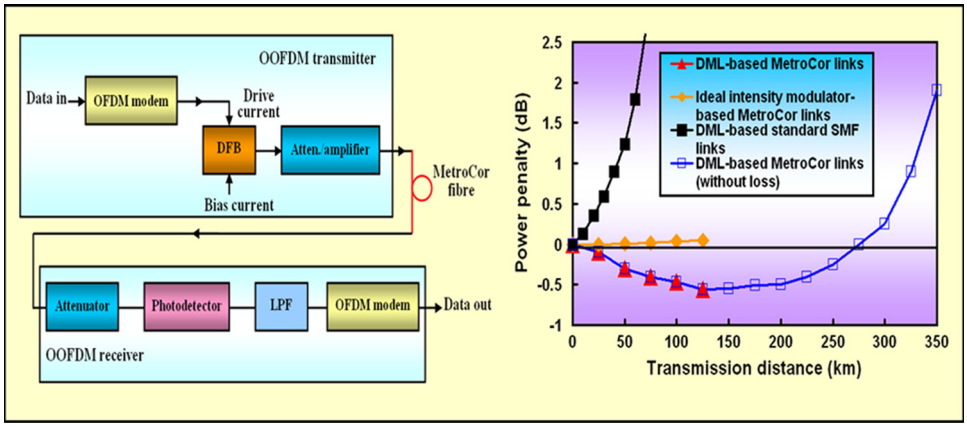

DOI: 10.1109/JPHOT.2010.2050464
1943-0655/$26.00 ©2010 IEEE

Negative Power Penalties of Optical OFDM Signal Transmissions in Directly Modulated DFB Laser-Based IMDD Systems Incorporating Negative Dispersion Fibers

X. Zheng, X. Q. Jin, R. P. Giddings, J. L. Wei, E. Hugues-Salas, Y. H. Hong, and J. M. Tang

School of Electronic Engineering, Bangor University, LL57 1UT Bangor, U.K.

DOI: 10.1109/JPHOT.2010.2050464
1943-0655/$26.00 ©2010 IEEE

Manuscript received April 26, 2010; revised May 8, 2010; accepted May 10, 2010. Date of publication May 18, 2010; date of current version June 18, 2010. This work was supported in part by the European Community's Seventh Framework Program (FP7/2007-2013) within the project ICT ALPHA under Grant agreement no. 212 352 and in part by The Royal Society Brian Mercer Feasibility Award. The work of X. Zheng, X. Q. Jin, and J. L. Wei was supported by the School of Electronic Engineering, Bangor University. Corresponding author: J. M. Tang (e-mail: j.tang@bangor.ac.uk).

Abstract: Detailed investigations of dynamic negative power penalty characteristics of optical orthogonal frequency division multiplexing (OOFDM) signal transmissions are undertaken, for the first time, in directly modulated distributed feedback (DFB) laser (DML)-based intensity modulation and direct detection (IMDD) systems incorporating negative dispersion fibers such as MetroCor fibers. Excellent agreements between numerical simulations and real-time experimental measurements are obtained over a wide diversity of transmission conditions of the aforementioned systems. The physical mechanism underpinning the occurrence of negative power penalties is the reduction in subcarrier intermixing impairment due to the compensation between DML positive frequency chirps and MetroCor negative chromatic dispersions. It is also shown that the negative power penalty is independent of both cyclic prefix and signal modulation format and, more importantly, controllable when adaptive modulation and/or appropriate adjustments of DML operating conditions are applied.

Index Terms: Orthogonal frequency division multiplexing (OFDM), power penalty, negative dispersion fiber, directly modulated laser, frequency chirp.

1. Introduction

With exponentially increasing end-users' demands for broadband services and the availability of enormous transmission capacities in core networks, existing access networks have become critical bottlenecks for fully utilizing the core network bandwidths to provide end-users with desired services [1]–[3]. To address such a challenge, great effort has been expended on exploring various techniques for enabling cost-effective, flexible, and "future-proof" next-generation passive optical networks (NG-PONs) [4]. Of those techniques, optical orthogonal frequency division multiplexing (OOFDM) has attracted extensive research and development interest [5]–[8], since OOFDM has a number of inherent and unique advantages including, for example, great potential for providing cost-effective technical solutions by fully exploiting the rapid advances in modern digital signal

processing (DSP) technology and considerable reduction in optical network complexity owing to its excellent resistance to dispersion impairments as well as adaptive and efficient utilization of channel spectral characteristics. Apart from the aforementioned advantages, OOFDM is also capable of offering, in both the frequency and time domains, hybrid dynamic allocation of broadband services among various end-users [6].

To develop cost-effective OOFDM NG-PONs, intensity modulation and direct detection (IMDD) [5], [7]–[11] is a very promising solution, as it is capable of offering further reductions in both the network complexity and the installation and maintenance cost without considerably compromising the system flexibility and performance robustness. In addition, compared to other intensity modulators such as conventional external intensity modulators, the use of directly modulated distributed feedback (DFB) lasers (DMLs) is also preferable due to their many salient advantages namely low cost, compactness, low power consumption, relatively small driving voltage, and high output power [9].

However, in DML-based IMDD OOFDM PONs utilizing standard single-mode fibers (SMFs) with positive chromatic dispersion parameters, the positive frequency chirps associated with typical DMLs significantly limit the maximum achievable OOFDM transmission performance [8]. In traditional non-return to zero (NRZ) DML-based IMDD transmission systems, use can be made of negative dispersion SMFs such as MetroCor fibers to compensate for the DML-induced positive frequency chirps, and negative power penalties have been observed experimentally at specific bit error ratios (BERs) [12], [13]. More importantly, such a dispersion compensation technique has also been confirmed to be very effective for OOFDM systems. We have experimentally demonstrated [10], [11] that net signal bit rates of 3 Gb/s 16-QAM-encoded, 4.5 Gb/s 64-QAM-encoded, and 5.25 Gb/s 128-QAM-encoded real-time OOFDM signals modulated by DMLs can be transmitted over 75 km, 25 km, and 25 km MetroCor SMFs, respectively, with respective negative power penalties of -2 dB, -0.5 dB, and -0.5 dB.

Given the fact that OOFDM has strong resilience to chromatic dispersion, the occurrence of negative power penalties in DML-based IMDD OOFDM MetroCor SMF systems raises three very interesting open questions listed as follows:

- What are the physical mechanisms underlying the observed negative power penalties?
- Does cyclic prefix contribute to such a phenomenon?
- What technical approaches may be adopted to control the effect?

The provision of answers to these three open questions is of great importance, as the answers enable us not only to gain an in-depth understanding of the IMDD OOFDM technique but also offer effective means for further maximizing the transmission performance of the systems of interest of the present paper. Therefore, this paper is dedicated to address, for the first time, such challenging issues.

In this paper, detailed investigations are undertaken, for the first time, to explore the dynamic negative power penalty characteristics of OOFDM signal transmissions over DML-based IMDD MetroCor systems. Excellent agreements between numerical simulations and our real-time experimental measurements [10], [11] are observed. This leads to the identification of the physical origin underpinning the negative power penalties: 1) in the electrical domain, the imperfect preservation of the OOFDM signal phase due to subcarrier intermixing upon square-law direct detection in the receiver and 2) the reduced subcarrier intermixing effect [7] due to a MetroCor fiber-induced reduction in DML modulated OOFDM signal phase. In addition, results also indicate that, for a given DML-based IMDD OOFDM MetroCor SMF system, the resulting negative power penalty is independent of both cyclic prefix and signal modulation format. Furthermore, it is also shown that the negative power penalty is controllable by applying adaptive modulation and/or variation in DML operating condition.

The paper is organized as follows. In Section 2, the considered transmission link model is outlined with special attention being given to the DML frequency chirp effect. In Section 3, parameters adopted in numerical simulations are presented and discussed in detail. In Section 4, extensive comparisons between numerical simulations and experimental results are made, based

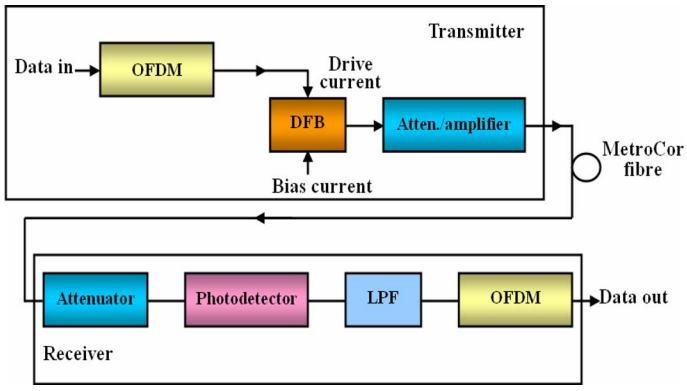

Fig. 1. Schematic illustration of DML-based IMDD OOFDM transmission systems. Atten.: attenuator; LPF: low-pass filter.

on which the physical origin of negative power penalties is identified. In addition, detailed discussions are also made of the impacts of cyclic prefix, adaptive modulation, signal modulation format, and DML operating conditions on the negative power penalty effect. Finally, this paper is summarized in Section 5.

2. Transmission Link Model

2.1. Transmission Link Diagram

Similar to those used in real-time experimental measurements [10], [11], the OOFDM transmission link considered here is a single-channel, DML-based IMDD MetroCor SMF system, as shown in Fig. 1, which is free from both chromatic dispersion compensation and in-line optical amplification. The transmission link consists of an OOFDM transmitter, an OOFDM receiver and MetroCor fibers in between. In the transmitter, an input binary data sequence is encoded by different modulation formats, which may vary from differential binary phase shift keying (DBPSK), differential quadrature phase shift keying (DQPSK), and 16 to 128-QAM. The encoded complex data are processed by a transmitter OFDM modem following the procedures described in [10], [11]. The procedures are outlined as follows: serial to parallel conversion, inverse fast Fourier transform (IFFT), cyclic prefix insertion, parallel to serial conversion, and digital to analog conversion. It should be pointed out that, at the input of the IFFT, the encoded original data (together with a zero-valued component) and their conjugate counterparts are arranged to satisfy Hermitian symmetry to produce a real-valued electrical OFDM signal. The electrical OFDM signal is first multiplexed with an optimum DC bias current, and then employed to directly drive the DML to generate an OOFDM signal at 1550 nm. After appropriately adjusting the output optical power, the OOFDM signal is coupled into the MetroCor fibers.

In the receiver, the optical signal occurring from an optical attenuator is detected using a square-law photo-detector. To recover the data, the low-pass-filtered electrical OFDM waveform is processed in a receiver OFDM modem by using an inverse process of the transmitter. Detailed descriptions of the processes outlined above have been reported in [10] and [11].

2.2. Theoretical DML Model and DML Frequency Chirp

2.2.1. DML Model

To simulate the characteristics of a DML, a lumped DFB model [14] is utilized, in which longitudinal mode spatial-hole burning, linear and nonlinear carrier recombination, and nonlinear

gain effects are taken into account. The output power and phase of the modulated optical signal are governed by [14]

$$\frac{dN}{dt} = \frac{I_d}{edwl} - \frac{N}{\tau_C} - BN^2 - CN^3 - G\frac{(N - N_t)}{1 + \varepsilon\phi}\phi \tag{1}$$

$$\frac{d\phi}{dt} = \frac{\Gamma G(N - N_t)}{1 + \varepsilon\phi}\phi + \zeta BN^2 - \frac{\phi}{\tau_P} \tag{2}$$

$$P = \chi w_v w_h h\nu \frac{\phi c}{2n_g} \tag{3}$$

$$\frac{d\Phi}{dt} = -\frac{\Gamma\eta(N - N_t)}{n_p} \tag{4}$$

$$\omega = \omega_0\left(1 - \frac{\Gamma\eta(N - N_t)}{n_p}\right) \tag{5}$$

where N is the carrier density, ϕ is the photon density, and P and Φ are the power and phase of the modulated optical signal at the optical frequency of ω with respect to a central frequency ω_0. I_d is the total electrical current injected into the active region of the laser with length l, width w, and thickness d, e is the electronic charge. τ_c is the linear carrier recombination lifetime. B is the bimolecular carrier recombination coefficient. C is the Auger carrier recombination coefficient. G is the linear optical gain coefficient. N_t is the transparency carrier density. ε is the nonlinear gain coefficient. Γ is the mode confinement factor. ζ describes the fraction of spontaneous emission that is emitted into the fundamental mode of the laser. τ_p is the photon lifetime. χ is the coupling efficiency from the laser chip to the SMF, w_v and w_h are the vertical and horizontal widths of the guided mode power distributions, h is the Planck's constant, c is the velocity of light in a vacuum, $h\nu$ is the photon energy. n_g is the group refractive index. n_p is the phase refractive index. η is the rate of refractive-index change with carrier density. In deriving (3) and (4), it is assumed that all photons reaching the exit facet of the DML are emitted and that the optical frequency can track the resonant frequency of the DFB cavity.

2.2.2. DML Frequency Chirp

Direct modulation of laser driving current introduces a nonlinear frequency chirp to the optical field. Based on (4) and (5), the DML frequency chirp Δv can be expressed as

$$\Delta v = -\frac{\omega_0\Gamma\eta(N - N_t)}{n_p} \tag{6}$$

As η is negative [14], the DML frequency chirp is, therefore, positive and varies with driving and bias currents and optical characteristics of the DFB laser.

It is well known that the DML frequency chirp has two major elements, namely, the transient frequency chirp and the adiabatic frequency chirp. Their relationships are given by [9]

$$\Delta v = \frac{\alpha}{4\pi}\left(\frac{1}{P}\frac{dP}{dt} + \kappa P\right) \tag{7}$$

where α is the linewidth enhancement factor, and κ is the adiabatic frequency chirp coefficient. The first term in (7) denotes the transient frequency chirp, which is proportional to the time-variation of an optical signal waveform, while the second term denotes the adiabatic frequency chirp, which depends on the instantaneous optical signal waveform.

To explicitly identify the origin of the frequency chirp associated with the theoretical DML model adopted here, (2) is rewritten as

$$\frac{1}{\phi}\frac{d\phi}{dt} = \frac{\Gamma G(N - N_t)}{1 + \varepsilon\phi} + \frac{\zeta BN^2}{\phi} - \frac{1}{\tau_P}. \tag{8}$$

TABLE 1

Parameters for different modulation formats

Optimum simulation parameters			
Modulation format	16QAM	64QAM	128QAM
Bias current of DML	35mA	37mA	39mA
Peak-to-peak drive current of DML	12.7mA	12.7mA	12.7mA
Clipping ratio	13.8dB	13.5dB	11dB

Given the fact that an electrical OFDM signal has a noise-like waveform and a very small extinction ratio (typically $<$ 1 dB) [15], for a DFB subject to optimum operating conditions, in (8), we have $1 + \varepsilon\phi \approx 1$ and a negligible second term which takes into account the contributions from spontaneous emission. Moreover, the last term accounting for cavity loss does not considerably alter the dynamic frequency properties of the DML within the 3-dB modulation bandwidth region. Taking into account the above analysis and (3), (8) can be simplified and has the form

$$\frac{1}{P}\frac{dP}{dt} = \frac{1}{\phi}\frac{d\phi}{dt} = \Gamma G(N - N_t). \tag{9}$$

Comparing between (6), (7), and (9), it can be seen that the transient frequency chirp plays a dominant role in determining the DML chirp characteristics in OOFDM transmission systems.

2.3. Models for Other Components

The propagation of OOFDM signals over MetroCor fibers is modeled using widely adopted split-step Fourier method [16]. The effects of loss, chromatic dispersion, and the optical power dependence of refractive index are included in the MetroCor fiber model. In addition, the effect of Kerr nonlinearity-induced phase noise to intensity noise conversion is also considered upon direct photon detection in the receiver.

In the p-i-n photo-detector model, both shot noise and thermal noise are considered, which are simulated following the procedure similar to that present in [17].

The validity of the theoretical fiber and PIN models has been confirmed in [7], [8], and [15].

3. Simulation Parameters

In this section, the parameters adopted in numerical simulations are discussed in detail. Throughout this paper, all the parameters listed below are utilized as default ones unless addressed explicitly in the corresponding text when necessary.

In simulating OFDM modems, the parameter values identical to those utilized in the experiments [10], [11] are adopted, which include 32 subcarriers with 15 conveying user data in the positive frequency bins, a cyclic prefix parameter of 25%, and an ADC/DAC with a 2 GS/s sampling rate and 8-bit quantization. According to the aforementioned parameters, the electrical OFDM signal has a bandwidth of 1 GHz. For different signal modulation formats, the optimum DML bias currents, peak-to-peak driving currents, and signal clipping ratios identified in the real-time experiments [10], [11] are also considered, which are summarized in Table 1. In addition, the experimentally measured DAC frequency response is also included, which has about 5 dB roll-off within the signal bandwidth region.

In numerical simulations, the following system parameters adopted in the experiments [10], [11] are also taken, which are a 7-dBm optical power launched into a SMF system, a noise equivalent power density of 27 pw$/\sqrt{\text{Hz}}$, and a responsivity of 0.91 A/W for the PIN.

All the parameter values employed in simulating the DFB laser are listed in Table 2. To obtain these parameter values, fitting of the experimental measurements with numerical results are

TABLE 2

DFB parameters

DFB	
Symbol	Value
l	300 μm
w	2 μm
d	0.033 μm
τ_c	10 ns
B	1×10^{-16} m^3/s
C	6.5×10^{-41} m^6/s
G	1.1×10^{-12} m^3/s
N_t	1.5×10^{24} m^{-3}
ε	7.4×10^{-23} m^{-3}
Γ	0.07
τ_p	3.6 ps
n_g	3.7
n_p	3.2203
w_v	0.47 μm
w_h	1.80 μm
η	-1.38×10^{-26} m^{-3}
ζ	1×10^{-5}
χ	37%

undertaken. All the parameter values which are not exactly known are initially taken from the literature [14], [18] and subsequently adjusted within reasonable limits to obtain the best fit with all the experimental results. It is also worth mentioning that, by adopting the DML parameters in Table 2, the DML model can give rise to a DFB threshold current of about 27 mA, and corresponding to this, an output optical power is approximately -30 dBm. The 3-dB modulation bandwidth is approximately 10 GHz. Such characteristics are very similar to those measured in the experiments [10], [11].

Finally, in simulating the MetroCor fibers, their typical parameter values at a wavelength of 1550 nm are employed, which are a dispersion parameter of -7.6 ps$/$(km $\cdot$ nm), a dispersion slope of 0.1 ps$/$(km $\cdot$ nm^2), a linear loss of 0.2 dB/km, an effective area of 70 μm^2, and a Kerr coefficient of 2.35×10^{-20} m^2/W.

4. Results and Discussions

To rigorously verify the developed transmission link model, extensive comparisons between numerical simulations and experimental measurements are first made in various transmission systems. After that, detailed numerical results are presented to explore the physical origin of the observed negative power penalties and subsequently identify effective technical approaches that can be used to improve the DML-based IMDD OOFDM system performance.

Throughout this paper, the power penalty is defined, for achieving a BER of 1×10^{-3}, as the received optical power difference between a full transmission link of a specific transmission distance and the corresponding optical back-to-back system configuration. It should be pointed out that, for fair comparisons between numerical simulations and experimental measurements, both the power penalty definition and its corresponding calculation procedure used in numerical simulations are identical to those reported in [10] and [11]. Here, it is also worth mentioning that, in numerical simulations, the BER is obtained by directly counting errors occurring within 2000 OFDM symbols, which, prior to being transmitted over a SMF link, are oversampled to give a total number of sample

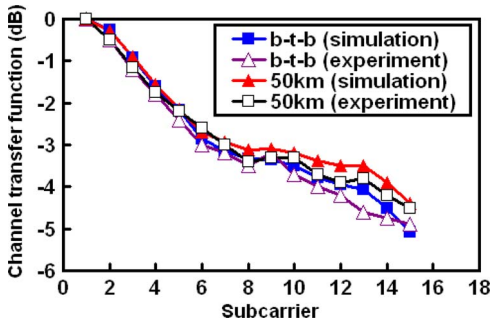

Fig. 2. Comparisons of normalized channel transfer functions for different DML-based IMDD link configurations.

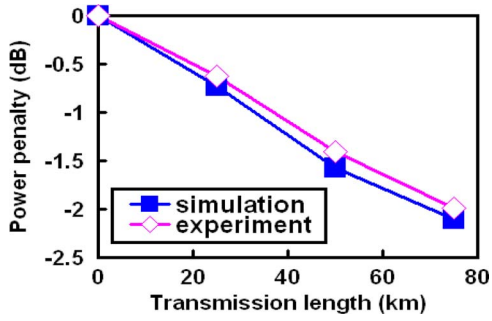

Fig. 3. Comparisons of power penalty versus transmission distance for 16-QAM-encoded OOFDM signals of net signal bit rates of 3 Gb/s.

points of 512488 per data sequence. Similar to those reported in [10] and [11], net OOFDM signal bit rates are used in describing the system transmission capacity. For all results presented in this section, 16-QAM is considered across all the subcarriers within an OFDM symbol in both numerical simulations and experimental measurements, except that, in Fig. 4 (see Fig. 7), different signal modulation formats (adaptive signal modulation) are employed.

4.1. Comparisons Between Numerical and Experimental Results

For optical back-to-back and DML-based 50-km MetroCor IMDD links, comparisons of their normalized channel transfer functions (CTFs) measured from the input of the IFFT in the transmitter and the output of the FFT in the receiver are shown in Fig. 2. It can be seen in Fig. 2 that, for all the cases considered, the simulated CTFs are in good agreement with the experimental results. The rapid CTF decays of approximately 5 dB within the signal spectral region are mainly attributed to the DAC due to its output filtering and inherent sin(x)/x response. In comparison with the optical back-to-back case, the slightly up-shifted 50 km CTFs corresponding to high frequency subcarriers are a direct result of the compensation between the positive transient frequency chirp associated with the DML and the negative chromatic dispersion associated with the MetroCor fiber. This behavior contrasts sharply with the long transmission distance-induced CTF narrowing effect in standard SMF IMDD systems [15].

Comparisons of transmission distance-dependent power penalties are plotted in Fig. 3, where excellent agreements between the simulated results and experimental measurements are observed for transmission distances of up to 75 km MetroCor SMFs. With increasing transmission length, the power penalty decreases to a value as low as -2 dB for 75 km.

The power penalty as a function of OOFDM signal bit rate for 25-km MetroCor fibers is shown in Fig. 4, where the net signal bit rates of 3 Gb/s, 4.5 Gb/s, and 5.25 Gb/s are achieved by different

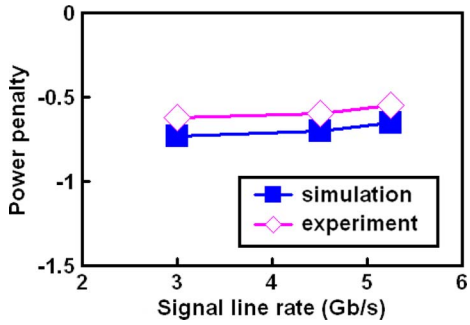

Fig. 4. Power penalties versus signal line rate obtained for different net signal line rates for 25-km MetroCor systems.

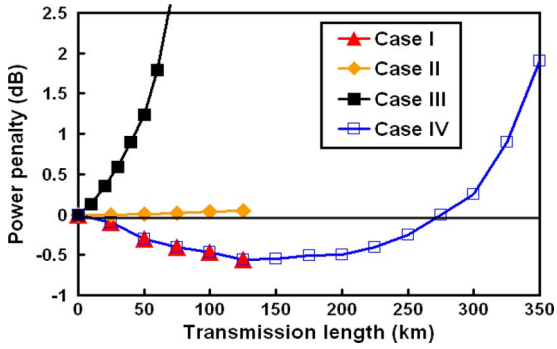

Fig. 5. Power penalty versus transmission distance for different link configurations. Case I: DML-based MetroCor links, Case II: ideal intensity modulator-based MetroCor links, Case III: DML-based standard SMF links. Case IV: DML-based MetroCor links without considering fiber linear losses.

signal modulation formats of 16-QAM, 64-QAM, and 128-QAM, respectively. Once again, the simulated results agree very well with the experimental observations. As expected from Fig. 3, in Fig. 4, a power penalty of approximately -0.6 dB is shown, which is almost independent of signal bit rate. It should be noted that the signal bit rate-independent negative power penalty behaviors also occur for OOFDM signals of higher signal bit rates. Numerical simulations show that power penalties of approximately -0.6 dB are obtainable for net signal bit rates of up to 30 Gb/s when 12.5GS/s DACs/ADCs are considered in 25-km MetroCor IMDD systems involving DMLs operating under conditions identical to those adopted in Fig. 4.

The aforementioned excellent agreements between the numerical simulations and the experimental measurements for a wide diversity of different systems strongly confirm the validity of the theoretical link model developed here. The link model can, therefore, serve as an excellent base for further exploration of the physical origin and dynamic characteristics of negative power penalties observed in such systems.

4.2. Physical Origin of Negative Power Penalty

To explore the physical origin of the negative power penalties observed in DML-based IMDD OOFDM MetroCor systems, Fig. 5 is plotted, where the transmission distance-dependent power penalties are given for various IMDD link configurations: Case I: DML-based MetroCor links; Case II: ideal intensity modulator-based MetroCor links; Case III: DML-based standard SMF links, and Case IV: DML-based MetroCor links, without considering fiber linear losses. In obtaining Fig. 5, a 38-mA bias current is employed for all the cases. For Case I and Case II, the maximum transmission distances of 125 km occur due to the fact that the received optical signal powers are too low to achieve total channel BERs of 1×10^{-3}.

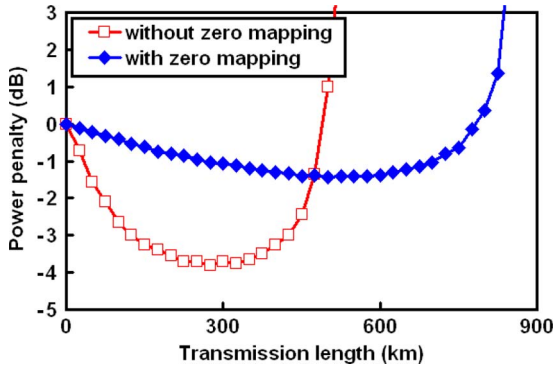

Fig. 6. Reduced subcarrier intermixing effect on power penalty.

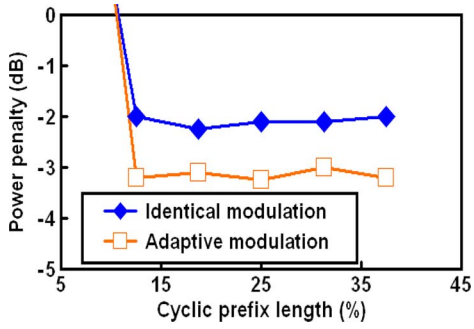

Fig. 7. Cyclic prefix dependent power penalty for different modulation schemes over 75-km MetroCor fibers.

Comparisons between the different cases considered in Fig. 5 show that only the co-existence of the DML and MetroCor fibers in Case I and Case IV leads to the occurrence of negative power penalties, whose values depend upon transmission distance. This implies that the negative power penalty is a direct result of the negative dispersion fiber-enabled compensation of the DML positive transient frequency chirp. Based on Fig. 5, the physical mechanisms behind the negative power penalty can be explained as follows: The optical-domain OOFDM signal phase cannot be preserved perfectly in the electrical domain due to subcarrier intermixing upon square-law photon detection in the receiver. As the unwanted subcarrier intermixing effect decreases with decreasing the optical phase at the input facet of the PIN, thus the MetroCor fiber-induced reduction in the DML-modulated OOFDM signal phase gives rise to the observed negative power penalty. Whilst, for coherent OOFDM MetroCor transmission systems, the OOFDM signal phase can be preserved perfectly in the electrical domain, no negative power penalties exist. This is verified by our numerical simulations, even when the optical phases identical to those corresponding to the IMDD cases are introduced into the coherent OOFDM signals.

The above physical explanations imply that a partial elimination of the subcarrier intermixing effect should be able to increase the obtained power penalty and simultaneously extend the transmission distance over which the minimum power penalty is observed. This is verified in Fig. 6, in obtaining which, to partly eliminate the subcarrier intermixing effect, zero-mapping of the first eight subcarriers close to the optical carrier is performed, and other parameter values identical to those used in Fig. 3 are adopted without considering the fiber linear loss effect.

4.3. Impacts of Adaptive Modulation and Cyclic Prefix on Negative Power Penalty

As the cyclic prefix does not considerably affect the subcarrier intermixing effect occurring in the receiver, a cyclic prefix-independent negative power penalty is thus observed, as seen in Fig. 7,

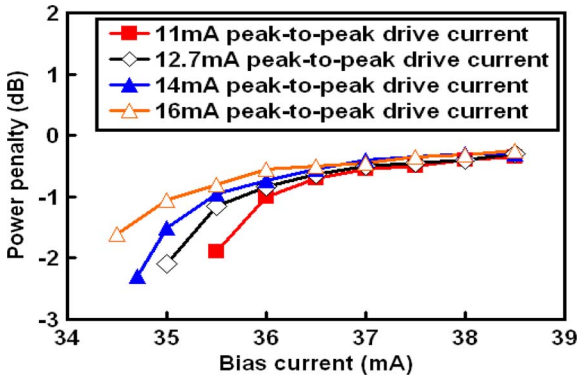

Fig. 8. DML operating condition-dependent power penalty.

for a transmission distance of 75 km. However, for cyclic prefix parameters of $< 6.25\%$, the cyclic prefix lengths are too short to compensate for the fiber chromatic dispersion effect, thus giving rise to sharply increased power penalty shown in Fig. 7. In addition, power penalty comparisons between identical modulation and adaptive modulation are also presented in Fig. 7. For the adaptive modulation case, a DQPSK (32-QAM) modulation format is taken on subcarriers experiencing a low (high) SNR to ensure that the resulting total channel BER remains at $< 1 \times 10^{-3}$, and the net signal bit rate is still fixed at 3 Gb/s (corresponding to a cyclic prefix parameter of 25%). It can also be seen in Fig. 7 that, in comparison with identical modulation, the use of adaptive modulation can further reduce the power penalty by about 1 dB. This is because adaptive modulation has better tolerance to the subcarrier intermixing effect owing to the assignment of different signal modulation formats on individual subcarriers experiencing different SNRs.

4.4. DML Operating Condition-Dependent Negative Power Penalty

Since the DML frequency chirp characteristics strongly depend on DML operation conditions including bias currents and peak-to-peak driving currents [14], the DML operating condition-dependent power penalty is thus seen in Fig. 8, where a 75-km MetroCor fiber is considered. It is shown in Fig. 8 that, for a fixed peak-to-peak driving current, a reduction in bias current can reduce the power penalty, resulting from the low bias current-induced increase in the DML frequency chirp effect. A reduction in bias current also produces a low optical output power and introduces strong unwanted signal clipping-induced waveform distortions to the modulated optical signals. These two effects significantly worsen the signal transmission performance and subsequently give rise to total channel BERs of $> 1 \times 10^{-3}$, even for optical back-to-back links. Thus, for a specific peak-to-peak driving current, a minimum bias current occurs, corresponding to which a minimum power penalty is observed.

On the other hand, over the low bias current region, the power penalty increases with increasing peak-to-peak driving current, as shown in Fig. 8. This is due to the enhanced signal clipping effect associated with the large peak-to-peak driving currents employed, as under such conditions, the signal clipping effect plays an important role in determining the system transmission performance. In addition, a low peak-to-peak driving current also requires a relatively high bias current to maintain the optical output power at an acceptable level, thus resulting in a minimum power penalty occurring in a relatively high bias current region, as shown in Fig. 8. It can also be seen in Fig. 8 that, for bias currents of > 37 mA, the power penalty differences among various peak-to-peak driving currents are negligible, this implies that, over such a bias current region, the DML frequency chirp is sufficiently small.

From the above analysis, it can be seen that the obtained negative power penalty is controllable when appropriate adjustments of DML operating conditions are applied.

5. Conclusion

Dynamic negative power penalty characteristics of OOFDM signal transmissions in DML-based IMDD MetroCor systems have been investigated in detail, and excellent agreements between numerical simulations and experimental measurements have been obtained for a wide diversity of system conditions. Based on a rigorously verified comprehensive theoretical transmission link model, the physical origin of the observed negative power penalties has been identified, i.e., the reduction in subcarrier intermixing impairment in the receiver due to the compensation between the DML positive frequency chirp and the MetroCor negative chromatic dispersion. Results have also shown that the negative power penalty is independent of cyclic prefix and signal modulation format and controllable when adaptive modulation and/or variations in DML operating conditions are applied.

References

[1] P. W. Shumate, "Fiber-to-the-home: 1977-2007," *J. Lightwave Technol.*, vol. 26, no. 9, pp. 1093–1103, May 2008.
[2] K. Iwatsuki and J.-I. Kani, "Application and technical issues of wavelength-division multiplexing passive optical networks with colorless optical network units," *J. Opt. Commun. Netw.*, vol. 1, no. 4, pp. c17–c24, Sep. 2009.
[3] B. O. Obele, M. Iftikhar, S. Manipornsut, and M. Kang, "Analysis of the behaviour of self-similar traffic in a QoS-aware architecture for integrating WIMAX and GEPON," *J. Opt. Commun. Netw.*, vol. 1, no. 4, pp. 259–273, Sep. 2009.
[4] M. Hajduczenia and H. J. A. da Silva, "Next generation PON systems—Current status," in *Proc. ICTON*, 2009, pp. 1–8, Paper Tu.B5.2.
[5] T.-N. Duong, N. Genay, M. Ouzzif, J. L. Masson, B. Charbonnier, P. Chanclou, and J. C. Simon, "Adaptive loading algorithm implemented in AMOOFDM for NG-PON system integrating cost-effective and low bandwidth optical devices," *IEEE Photon. Technol. Lett.*, vol. 21, no. 12, pp. 790–792, Jun. 2009.
[6] D. Qian, N. Cvijetic, J. Hu, and T. Wang, "108 Gb/s OFDMA-PON with polarization multiplexing and direct detection," *J. Lightwave Technol.*, vol. 28, no. 4, pp. 484–493, Feb. 2010.
[7] J. L. Wei, X. L. Yang, R. P. Giddings, and J. M. Tang, "Colourless adaptively modulated optical OFDM transmitters using SOA as intensity modulator," *Opt. Express*, vol. 17, no. 11, pp. 9012–9027, May 2009.
[8] J. M. Tang and K. A. Shore, "30 Gb/s signal transmission over 40-km directly modulated DFB-laser-based single-mode-fiber links without optical amplification and dispersion compensation," *J. Lightwave Technol.*, vol. 24, no. 6, pp. 2318–2327, Jun. 2006.
[9] J. J. Yu, Z. S. Jia, M. F. Huang, M. Haris, P. N. Ji, T. Wang, and G. K. Chang, "Applications of 40-Gb/s chirp managed laser in access and metro networks," *J. Lightwave Technol.*, vol. 27, no. 3, pp. 253–265, Feb. 2009.
[10] X. Q. Jin, R. P. Giddings, and J. M. Tang, "Real-time transmission of 3 Gb/s 16-QAM encoded optical OFDM signals over 75 km SMFs with negative power penalties," *Opt. Express*, vol. 17, no. 17, pp. 14 574–14 585, Aug. 2009.
[11] X. Q. Jin, R. P. Giddings, E. Hugues-Salas, and J. M. Tang, "Real-time demonstration of 128-QAM-encoded optical OFDM transmission with a 5.25 bit/s/Hz spectral efficiency in simple IMDD systems utilizing directly modulated DFB lasers," *Opt. Express*, vol. 17, no. 22, pp. 20 484–20 493, Oct. 2009.
[12] J. A. P. Morgado and A. V. T. Cartaxo, "Directly modulated laser parameters optimization for metropolitan area networks utilizing negative dispersion fibre," *IEEE J. Sel. Topics Quantum Electron.*, vol. 9, no. 5, pp. 1315–1324, Sep./Oct. 2003.
[13] I. Tomkos, B. Hallock, I. Roudas, R. Hesse, A. Boskovic, J. Nakano, and R. Vodhanel, "10-Gb/s transmission of 1.55-μm directly modulated signal over 100 km of negative dispersion fiber," *IEEE Photon. Technol. Lett.*, vol. 13, no. 7, pp. 735–737, Jul. 2001.
[14] J. M. Tang, P. M. Lane, and K. A. Shore, "High-speed transmission of adaptively modulated optical OFDM signals over multimode fibres using directly modulated DFBs," *J. Lightwave Technol.*, vol. 24, no. 1, pp. 429–441, Jan. 2006.
[15] J. L. Wei, A. Hamié, R. P. Giddings, and J. M. Tang, "Semiconductor optical amplifier-enabled intensity modulation of adaptively modulated optical OFDM signals in SMF-based IMDD systems," *J. Lightwave Technol.*, vol. 27, no. 16, pp. 3678–3688, Aug. 2009.
[16] G. P. Agrawal, *Nonlinear Fibre Optics*. New York: Academic, 1995.
[17] G. P. Agrawal, *Fibre-Optic Communication Systems*. New York: Wiley, 1997.
[18] J. E. A. Whiteaway, G. H. B. Thompson, A. J. Collar, and C. J. Armistead, "The design and assessment of $\lambda/4$ phase-shifted DFB laser structures," *IEEE J. Quantum Electron.*, vol. 25, no. 6, pp. 1261–1279, Jun. 1989.